FABRICATION OF SILVER NANOPARTICLES IN POMEGRANATE SEED OIL WITH THERMAL PROPERTIES BY LASER ABLATION TECHNIQUE

A. R. SADROLHOSSEINI[a], S. A. RASHID[a*], A.S.M. NOOR[b,c],
A. KHARAZMI[d], L. A. MEHDIPOUR[e]
a *Materials Processing and Technology Laboratory, Nanomaterials and
Nanotechnology Group, Institute of Advanced Technology, Universiti Putra
Malaysia, 43400UPM, Serdang, Selangor.*
b *Wireless and Photonic Network Research Center of Excellence (WiPNET),
Faculty of Engineering, University Putra Malaysia, 43400 UPM Serdang,
Selangor, Malaysia.*
c *Department of Computer and Communications System Engineering, Faculty of
Engineering, University Putra Malaysia, 43400 UPM Serdang, Selangor,
Malaysia.*
d *School of Chemistry, University of New South Wales, Kensington, NSW 2052,
Australia*
e *Department of Radiology, Faculty of Paramedical, Rafsanjan University of
Medical Sciences, Rafsanjan, Iran.*

Silver nanoparticles were fabricated in pomegranate seed oil using laser ablation technique. A silver plate was ablated for 5 minutes, 10 minutes, 15 minutes and 20 minutes using Nd:YAG Q-Switched laser to prepare the nanofluid. The nanofluids were characterized using UV-visible, transmission electron microscopy and Fourier transform infrared spectroscopy, respectively. The silver nanoparticles were formed in spherical shape and particles size shifted from 21 to 2 nm with increasing the ablation time. The silver nanoparticles were capped by carboxylic groups ($-COO^-$) of the pomegranate seed oil. Moreover, the thermal effusivity of samples was measured using the photo-acoustic technique, and the thermal effusivity shifted from 0.095 $Ws^{1/2}cm^{-2}$ K^{-1} to 0.144 $Ws^{1/2}cm^{-2}K^{-1}$ that confirmed the silver nanoparticles enhanced the thermal properties of pomegranate seed oil. Consequently, the laser ablation techniques succeed to fabricate the silver nanoparticles in the pomegranate seed oil.

1. Introduction

Pomegranate (Punica granatum) seed oil (PGO) derives from pomegranate fruit and is about the 20% of seed weight. PGO contains 8% saturated, 10% monosaturated, 10% disaturated, and about 70% conjugated acid [1]. PGO consists of rare conjugate linoleic acid isomer punicic acid, octadecatrienoic, linoleic acid, stearic acid, and palmitic acid [2]. Pomegranate and PGO have been utilized worldwide for diets and medicine [3, 4]. PGO has an antioxidant effect [5], an anti-inflammatory effect [6], and is nontoxic [7]. PGO has been used for possible skin cancer chemopreventive efficacy in mic [8]. Silver nanoparticles (Ag-NPs) are used in many applications in biology, medicine, and industry because it's high potential to enhance the physical and thermal properties of materials [9]. Silver nanoparticles (Ag-NPs) have been synthesized in several media such as water, oil, pomegranate extract starch, and polymer based stabilizer [10]. Therefore,

---

*Corresponding author: suraya_ar@upm.edu.my

Chemical, biological and physical techniques are used to fabricate the Ag-NPs [11]. The Ag-NPs were formed by colloidal solutions form the reduction of Ag salts in chemical methods [11, 12]. Hence, the chemical fabrication of Ag-NPs in aqueous solution usually needs the reduction agents, metal precursors (Ag salt) and stabilizer agent [13, 14, and 15]. In the biological method, bacteria, fungi, yeasts or plants are used for reducing or stabilizing agent [16, 17]. In the physical methods Ag-NPs synthesize by evaporation-condensation [11, 18, and 19] which could be used to a tube furnace at atmospheric pressure. The disadvantages of these methods are the tube furnace occupies a large space, consumes a great deal of energy and require a lot of time to achieve thermal stability. The second physical method is using a small ceramic heater. This method is suitable for high concentration and small Ag-NPs [19]. A thermal-decomposition is other method for preparation of Ag-NPs in powder form. The Ag-NPs were produced by decomposition of Ag+-oleate complex [11, 20]. The complex is prepared by the interaction of $AgNO_3$ and sodium oleate in water solution that is not compatible for Ag-NPs preparation in oil. The arc discharged technique is a method for preparation of Ag-NPs in water based solution without surfactant [21]. In this method, the silver wire is immersed in deionized water as electrodes which is disadvantage for preparation of Ag-NPs in compare with oil because the electrical conductivity of oil depends on fatty acid components [22] and is not constant. Recently, laser ablation in liquid has become a versatile and green technique to prepare the silver nanoparticles in aqueous solution [23, 24, 25]. In this method, a pulsed laser interacts with the surface of the silver target, and during the irradiation of silver plates [26, 27], the nanoparticles release inside the liquids [28] without presence of surfactant and other chemical agent. The advantages of the laser ablation technique are simple setup, no adducts, no counter ions and no residues from the reducing agents [28]. Moreover the nanoparticles are synthesized by single step inside the liquids, and the greatest advantage is that, the particle size and concentration of NPs are controlled by using the ablation time [29].

The main application of PGO is in skin care and dermatology, the thermal effusivity was used to measure the thermal properties of PGO-Ag-NPs. Thermal effusivity ($\alpha = \sqrt{k\rho c_p}$) is based on thermal impedance which is able to measure the heat exchange of sample with surroundings. Thermal effusivity (TE) is proportional to second root of thermal conductivity (k), density (ρ) and heat capacity (c_p) that are significant thermal parameters to explain the thermal properties of nano-materials [30]. In addition, TE is a non-destructive, fast and reliable methods to measure the thermal properties of human skin for understanding the thermophysical properties of skin with contact the materials [31, 32, 33, and 34].

In this paper, Ag-NPs in PGO (PGO-Ag-NPs) were synthesized by the laser ablation technique. The identification of the silver nanoparticles, the capped effect of PGO on the nanoparticle formation and the particle size distribution were investigated by using UV-Visible spectrum, Fourier transform infrared spectroscopy (FT-IR) and transmission electron microscopy (TEM), respectively while the thermal effect of PGO and PGO-Ag-NPs were determined by the photo-acoustic technique.

2. Material and methods

2.1. Laser ablation setup

Fig. 1 shows the laser ablation setup. This setup a pulsed Q-switched Nd:YAG laser (Spectra laser system), a lens (f=300 mm), a glass cube cell, a silver plate (Sigma-Aldrich, 99.99% purity), and a magnetic stirrer. Prior to the try out, the silver plate has been cleaned by means of the ultrasonic bath during 15 minutes. The silver plate was then immersed in 20 ml of pomegranate seed oil (BOTANICAL BEAUTY CO.) and irradiated in various ablation times. A laser beam with specification of 40 Hz repetition rate, 1200 mJ/pulse, and 10 ns in 532 nm wavelength was used to ablate the silver plate for a duration of 5, 10, 15 and 20 minutes.
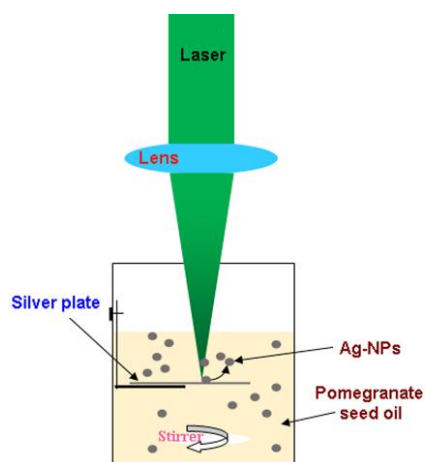
Fig. 1. Laser ablation setup consists of a Nd:YAG laser, a lens (300 mm), a silver plate,
and a magnetic stirrer. The silver plate was immersed in PGO and ablated for
5min,10min, 15min, and 20 min.

During the irradiation of the silver plate, the oil was magnetically stirred to disperse the nanoparticle inside the solution. The prepared samples were characterized by means of a UV-visible double beam spectrometer (Shimadzu), field emission transmission electron microscopy (FE-TEM, LEO 912AB), Fourier transform infrared spectroscopy (FT-IR, Spectrum 100, Perkin Elmer), and atomic absorption spectroscopy (AAS, S, series). The particle sizes were obtained through an analysis of the FE-TEM pattern using UTHSCA (Ver. 3) and SPSS software (ver. 18). Additionally, the photo-acoustic method was applied to assess the thermal effusivity of the nanofluids.

2.2. Photo-acoustic setup

The photo-acoustic setup consists of a He-Ne laser (75 mW, 632.8 nm), a chopper, a mirror, a fluid cell, a microphone, a pre amplifier, and a lock-in amplifier (Stanford Research) (see Fig 2). The chopper frequency was shifted from 20 Hz to 240 Hz to measure the thermal effusivity of the PGO and the PGO-Ag-NPs.
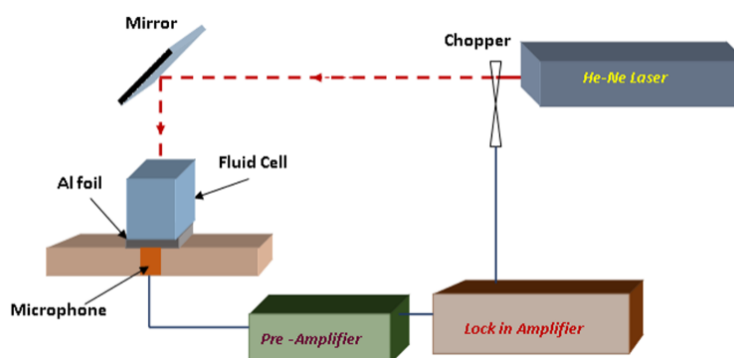

Fig. 2. Photoacoustic set-up measures the thermal effusivity of PGO, and PGO-Ag-NPs
contains a fluid cell, a He-Ne laser, a chopper, a mirror, a microphone, pre and Lock-in
amplifiers.

The experimental process was explained in ref. [35]. Briefly, the bottom of the fluid cell which contained the solution, was closed with an aluminum sheet with 0.017 mm thickness. In order to measure the thermal effusivity of PGO and PGO-Ag-NPs, the photo-acoustic signals were

registered using an electret microphone, connected to the pre- and lock- in amplifiers. The phase and amplitude of these signals were achieved as a function of the light beam modulation frequency. The thermal effusivity measurement was carried out for the empty fluid cell, water and ethylene glycol prior to measuring the thermal effusivity of PGO and PGO-Ag-NPs at room temperature.

3. Results and discussion

Fig. 3 illustrates the UV-Visible spectrum. The UV-visible spectrum of the pure PGO is the baseline. The peaks ascended from a plasmon resonance of the Ag-NPs, and they came into sight at 411 nm, 407 nm, 403 nm and 399 nm for 5 min, 10 min, 15 min and 20 min, respectively. By decreasing the particle size, the blue shift occurred. Intensity of the peak is depending on the centration of the Ag-NPs that shifted from 0.6 mg/l to 13 mg/l. Hence, the Ag-NPs formed in the PGO in spherical appearances.

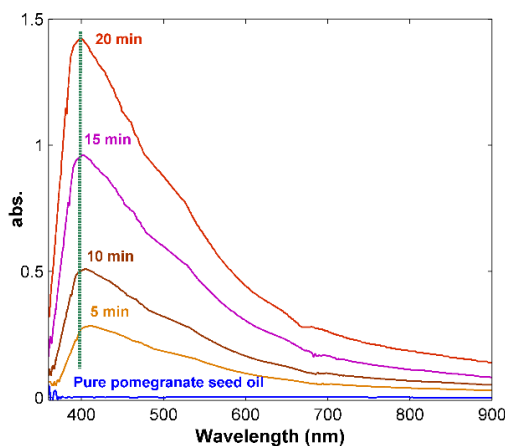*Fig. 3. The baseline of the UV-visible spectrum belongs to the pure PGO. The peak at 411nm, 407 nm, 403 nm and 399 nm appeared and the blue shift occurred to show that the particles size decreased when increasing the ablation time.*

Fig. 4 demonstrates the morphology of the Ag-NPs distributed in the PGO using the laser ablation technique. The FE-TEM pattern shows non-agglomerated as well as dispersion of the Ag-NPs with a spherical shape. The FE-TEM images were analyzed using UTHSCA (Ver. 3) software. The average particle size of the Ag-NPs for 5min, 10min, 15min and 20min was 21 nm, 14 nm, 10 nm and 2 nm, respectively. During the ablation of the silver plate, the Ag-NPs dispersed in the PGO using the magnetic stirrer, and the laser beam passed through the PGO. At first, the Ag-NPs formed through phase transition and nucleation, hence; crystals of the Ag cluster expanded from released silver atoms, and fatty acids of the PGO capped the Ag-NPs. Afterward, the laser beam interacted with the nanofluid (see Figure 5) and the Ag-NPs were ablated and broken to a small size. Therefore, the particle diameter decreased as the ablation time increased [28].
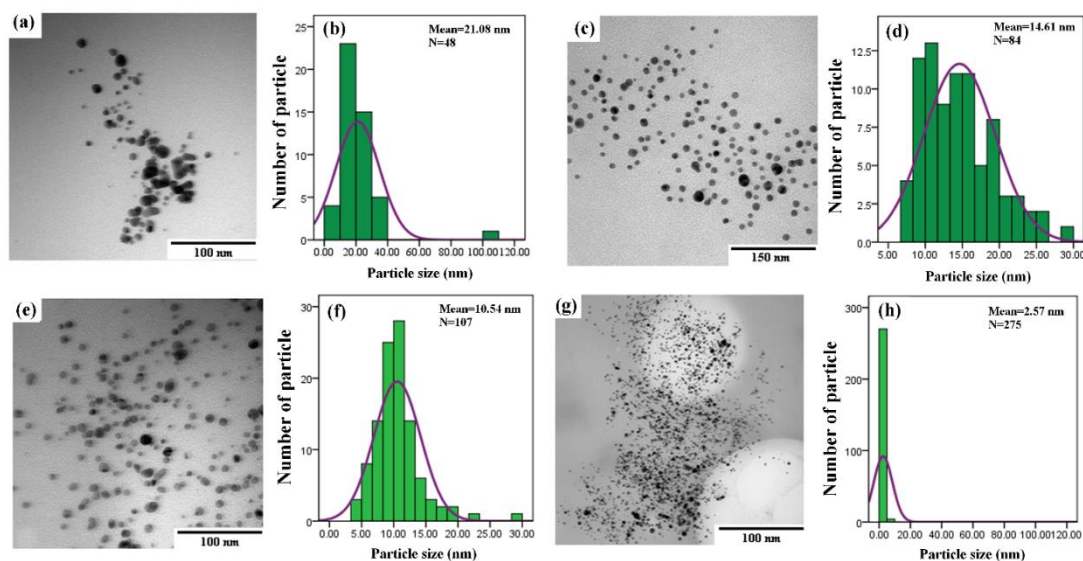
Fig. 4. FE-TEM images show the distribution of the Ag-NPs in the PGO. FE-TEM images and analysis for 5 , 10, 15 and 20 min were presented in (a), (b), (c), (d), (e), (f), (g) and (h) . The images were analyzed using UTHSCA (Ver. 3) software ((b), (d), (f) and (h)) and the average particles diameters are 21 nm, 14 nm, 10 nm, and 2 nm. The particle size decreases with an increase the ablation time in the range of 5 min to 20 min.
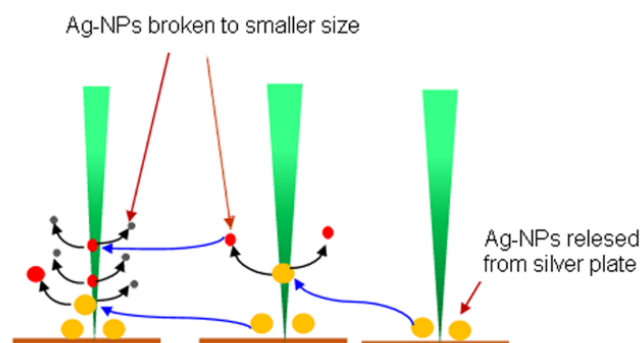

Fig. 5. At first, the laser beam ablated the silver nanoparticle, and the Ag-NPs formed in the PGO. Then, the laser beam ablates the silver plate and the Ag-NPs as well

Fig. 6 shows the FT-IR spectrum. This spectrum was recorded at a wavelength range of 280 cm^{-1} and 4000 cm^{-1}. The FT-IR spectrum was depicted as chemical structure before and after laser ablation of the silver plate. The FT-IR spectrum (Figure 6(a)) of the pomegranate seed oil was revealed at a =C-H stretching vibration at 3474.67cm^{-1}, 3008.69 cm^{-1}, CH$_2$ asymmetric and symmetric at 2923.38cm^{-1} and 2855.07cm^{-1} , and -C=C stretching ester carbonyl function group of triglyceride at 1743.31 cm^{-1}. Moreover, the peaks of 1457.55 cm^{-1}, 1371.05 cm^{-1}, 1234.91 cm^{-1}, 1158.72 cm^{-1} and 720 cm^{-1} corresponded to the CH$_2$ bending, -C-O stretching vibration, -C-O stretching and –CH$_2$ bending (sis –CH=CH- bending). The FT-IR spectrum after the ablation of the silver plate is demonstrated in Figure 6(b). The peaks at 3475.32 cm^{-1}, 3008.61 cm^{-1}, 2923.31 cm^{-1}, 1743.24 cm^{-1}, 1457.54 cm^{-1}, 1371.08 cm^{-1}, 1234.88 cm^{-1}, 1158.76 cm^{-1} and 720 cm^{-1} are related to the structure and components of the PGO. The peaks at the wavelengths of 1743.24 and 295 cm^{-1} was assigned to the C-O stretching vibration band of carboxylic acid groups (COOH) and silver nanoparticles, respectively. The peak at 1743.24 cm^{-1} shifted to 1788.78 cm^{-1} indicated a strong link between silver nanoparticles and COO^{-} of carboxylic acid groups. Figure 6(c) shows the mechanism of capping of Ag-NPs in PGO. The tail of carbonyl band capped the nanoparticle through the electron transfer from carboxylic group to Ag-NPs; hence the motion of molecules

impeded inside the particular area, and the entropy decrease [36, 37, and 38]. Therefore, the long hydrocarbons chain prevents the agglomeration of Ag-NPs.
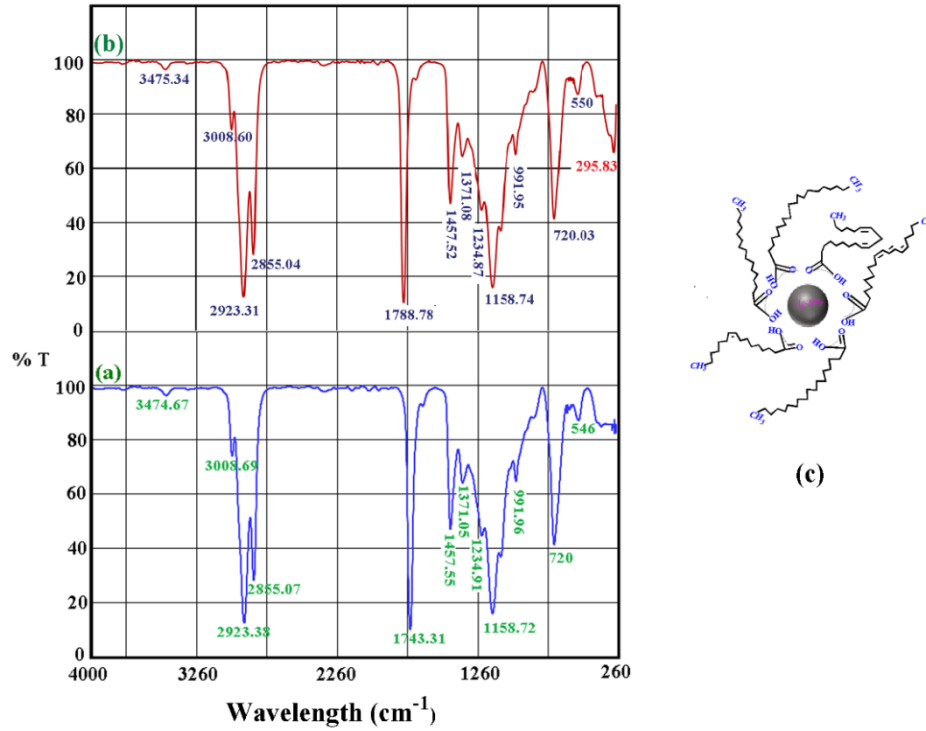

Fig. 6. a) The FT-IR result belongs to the pure PGO and shows the structure and the components of the oil. b) The FT-IR result for PGO-Ag-NPs shows the bonding of the Ag-NPs to COO⁻ . c) Ag-NPs was capped with carboxylic group of PGO.

To calculate the thermal effusivity, the Rosencwaig–Gersho (RG) theory was used to analyze the photo-acoustic signals. The amplitude of pressure fluctuations (δP) has been calculated as [35].

$$|\delta P| = \frac{P_1}{f^{P_2}\left(1 + \dfrac{P_3}{\sqrt{f}} + \dfrac{P_3^2}{\sqrt{2f}}\right)^{\frac{1}{2}}} \tag{1}$$

where

$$P_3 = \frac{2\varepsilon_s}{\varepsilon_{Al} l_{Al}}\left(\frac{\alpha_{Al}}{\pi}\right)^{\frac{1}{2}} \tag{2}$$

$\alpha_{Al}, \varepsilon_{Al}, l_{Al}$, ε_s and f are the thermal diffusivity, thermal effusivity, thickness of aluminum foil, thermal effusivity of the sample and modulation frequency, respectively. P_1 and P_2 are the adjustable parameters which have constant values. They were obtained from the Al foil signal as a function of the modulation frequency (f). P_1 and P_2 should be calculated from fit with the former data, using Equation (3), [39].

$$|\delta P_{Al}| = P_1 f^{P_2} \tag{3}$$

The parameters of aluminum foil such as a $\alpha_{Al}, \varepsilon_{Al}$ and l_{Al} were 2.36 cm²/s, 0017 Ws^{1/2}cm⁻² K⁻¹ and 0.99 mm, respectively. These parameters were used to attain the P_1 and P_2 using an empty closed bottom fluid cell.

Figures 7 shows the photo-acoustic signals that relate to the water and ethylene glycol for testing the setup. The thermal effusivity of the water and ethylene glycol were 0.1614 $Ws^{1/2}cm^{-2}K^{-1}$ and 0.0826 $Ws^{1/2}cm^{-2}K^{-1}$ which matched the literature [40, 41].
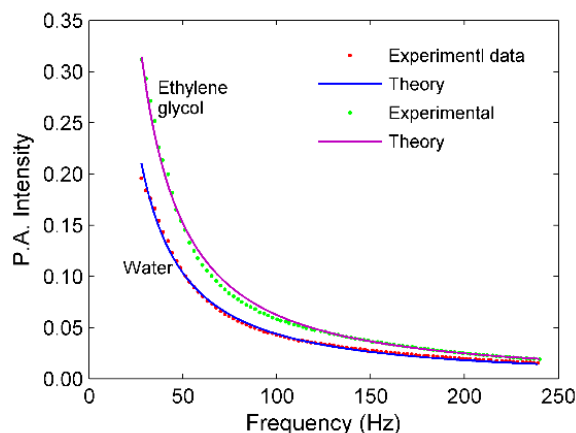

Fig. 7. The Photo-acoustic signal relates to water and ethylene glycol for testing the setup. P_1 and P_2 are 1.64956 and 344.94063, respectively.

The experiment was repeated for the PGO and the PGO-Ag-NPs. Figures 8 and 9 depict the photo-acoustic signals for the PGO and the PGO-Ag-NPs with different ablation time in the range of 5 min to 20 min, respectively. The equation (1) was fit to the experimental data (dotted) to obtain the P_3. Afterward, the thermal effusivity of the PGO and the PGO-Ag-NPs was calculated using equation (2). The results for the samples are sorted in Table 1.

As AAS results, the concentration of the Ag-NPs in the PGO for 5 min, 10 min, 15 min and 20 min ablation times were 0.6 ppm, 1.4 ppm, 4 ppm and 13 ppm, respectively. The volume fraction for the samples was calculated using equation [38]

$$V = \frac{V_p}{V_p + V_L} \qquad . \qquad (4)$$
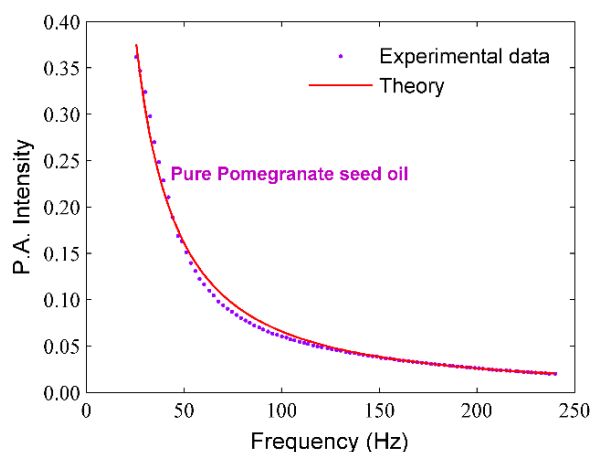

Fig. 8. Photo-acoustic signals to calculate the thermal effusivity of the PGO, and the adjustable parameters such as P_1, P_2 and P_3, are 1.64956, 344.94063, and 25.1, respectively.
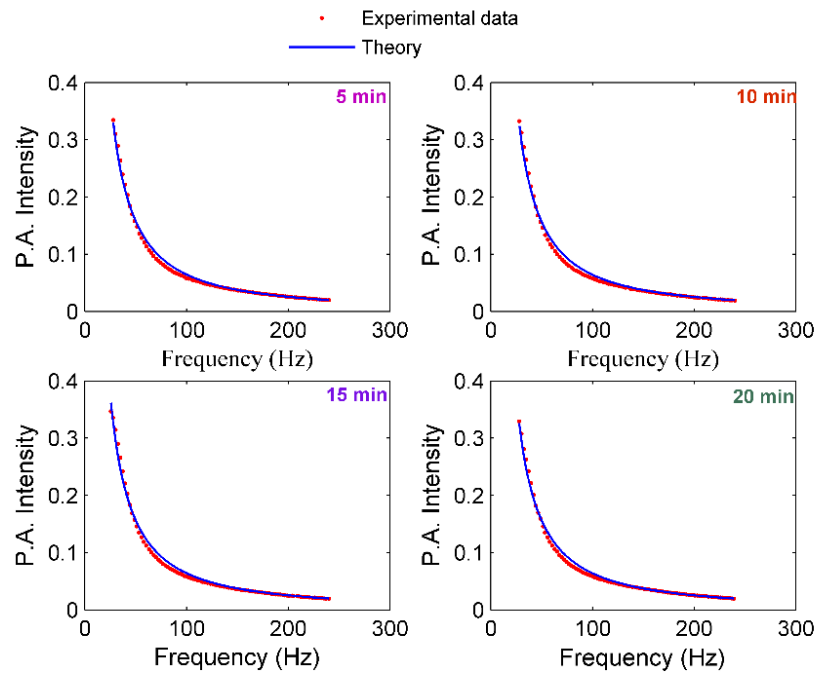
Fig. 9. Photo-acoustic signals for calculation of the PGO-Ag-NPs with different ablation times in the range of 5 min to 20 min. The adjustable parameters, P_1 and P_2 are 1.64956 and 344.94063, respectively. The P_3 for the PGO-Ag-NPs with different ablation times are sorted in Table 1.

Where V_L and V_p are the volume of the PGO and the volume of the Ag-NPs (m/ρ, where ρ and m are the mass density of the silver and the particles mass dispersed in the PGO, respectively). Hence, equation (5) was derived from a modification and a simplification of Equation (4) as follows:

$$V = \frac{C_{Particle}}{C_{Particle} + \rho},$$

(5)

where the $C_{Particle}$ are the concentrations of the Ag-NPs obtained from the AAS. The volume fraction of nanoparticles increased with an increase in the ablation time from 0.0057×10^{-5} to 0.1238×10^{-5} (see Table 1).

Table 1. The pertinent parameters of the samples.

Sample	P_3	Thermal effusivity ($Ws^{1/2}cm^{-2}K^{-1}$)	Concentration of Ag-NPs (ppm)	Volume fraction
Water	45.17	0.1614	-	-
Ethylene glycol	23.1	0.0826	-	-
Pure PGO	25.1	0.089	-	-
5min	26.6	0.095	0.6	0.0057×10^{-5}
10 min	27.9	0.099	1.4	0.0133×10^{-5}
15 min	30	0.107	4	0.0381×10^{-5}
20min	31.9	0.144	13	0.1238×10^{-5}

Fig. 4 depicted the number of particle will be increased more than five times, when the ablation time shifted from 5 min to 20 min. Figure 10 demonstrates the variation of thermal

effusivity versus to volume fraction. The thermal effusivity explains the exchange of heat with the environment which is in contact with the sample. When the concentration or volume fraction of the Ag-NPS is increased, the number of scattering centers (Ag-NPs) will be augmented inside the PGO-Ag-NPs. Hence, the ability of the PGO-Ag-NPs to exchange the heat with the environment is higher than pure PGO.
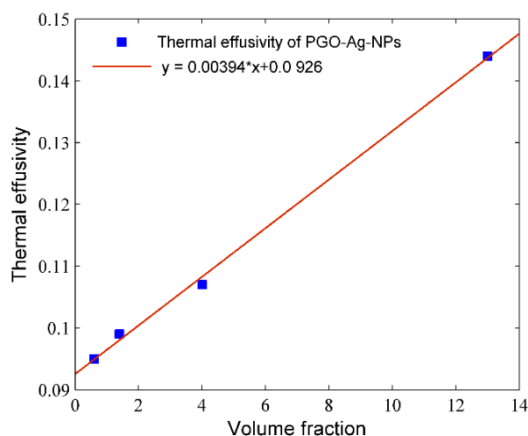

Fig. 10. Variation of thermal effusivity versus volume fraction is a linear form achieved from spline (R≈0.95).

4. Conclusions

The silver nanoparticle was dispersed in the PGO monotonous and capped with –COO⁻ of the carboxylic acid groups of fatty acid in PGO. The particle size decreased with an increase the ablation time and the ability of the PGO to exchange the heat to the environment was enhanced with Ag-NPs. Consequently, the PGO is a satisfactory stabilizer for dispersing the Ag-NPs using laser ablation.

References

[1] A.M. Goula, K.G.A. Adamopoulos, Food and Bioproducts processing, **90**, 639(2007).
[2] A. Fadavi, M. Barzegar, M.H. Azizi, J Food Comp. Anal. **19**, 676(2006).
[3] F. Balkwill, K.A. Charles, A. Mantovani, Cancer Cell, **7**, 211(2005).
[4] E.P. Lansky, R.A. Newman, J. Ethnopharmacology, **109**, 177(2007).
[5] P. Jing, S. T.Y. Haiming, Y. Sheng, M. Slavin, B. Gao, L. Liu, L. Yu, Food Chemistry **132**, 1457(2012).
[6] M. Spilmont, L. Léotoing, M.J. Davicco, P. Lebecque, S. Mercier, E. Miot-Noiraulte, P. Piletd, L. Riosh, Y. Wittrant, V. Coxam, Journal of Nutritional Biochemistry (2013) (in press).
[7] I.A.T.M. Meerts, C.M. Verspeek-Rip, C.A.F. Buskens, H. G. Keizer, J. Bassaganya-Riera, Z.E. Jouni, A.H.B.M. van Huygevoort, F.M.van Otterdijk, E.J. van de Waart, Food and Chemical Toxicology **47**, 1085(2009).
[8] J.J Hora, E.R. Maydew, E. P. Lansky, C. Dwivedi, J Med Food **6**, 157(2003).

[9] R. Zamiri, Z. Azmi, A.R. Sadrolhosseini, H. A. Ahangar, A.W. Zaidan, M.A. Mahdi, International Journal of Nanomedicine 6, 71(2011).

[10] M. Solgi, M. Taghizadeh, International Journal of Nanomaterials and Biostructures Available online at http://www.urpjournals.com

[11] Q. H. Tran, V. Q. Nguyen, A. Le, Adv. Nat. Sci.. Nanosci. Nanotechnol. **4**, 033001(2013).

[12] G. B. Khomutov, S. P. Gubin, Mater. Sci. Eng. C 22, 141(2002),

[13] S. F. Chen, H. Zhang, Adv. Nat. Sci.. Nanosci. Nanotechnol. 3, 035006(2012).

[14] T. M. D. Dang, T.T.T.Le, E. F. Blance, M. C. Dang; Adv. Nat. Sci.. Nanosci. Nanotechnol. **3**, 035004(2012).

[15] R. S. Patil, M. R. Kokate, C. L. Jambhale, S. M. Pawar, S. H. Han, S. S. Kolekar; Adv. Nat. Sci.. Nanosci. Nanotechnol. **3**, 015013 (2012).

[16] S. Prabhu, E. K Poulose, International Nano Letters **2**, 32(2012).

[17] L. Sintubin, W. Verstraete, N. Boon , Biotechnol. Bioeng. 109, 2422(2012).

[18] A. Gurav, T. Kodas, L. Wang, E. Kauppinen, J. Joutsensaari, Chem. Phys. Lett. **218**, 304(1994).

[19] M. M. Kholoud, A. El-Nour , A. Eftaiha , A. Al-Warthan, R. A.A. Ammar, Arabian Journal of Chemistry **3**, 135 (2013).

[20] D. K. Lee and Y. S. Kang, ETRI J. **26**, 252 (2004).

[21] D.C. Tien, K. H. Tseng, C.Y. Liao, J. C. Huang, T. T. Tsung, J. Alloys Compounds **463**, 408 (2008)

[22] www.machinerylubrication.com

[23] A. Fojtik, A. Henglein, Chemical Physics, **97**, 252 (1993).

[24] T. Tsuji, D.H. Thang, Y. Okazaki, M. Nakanishi, Y. Tsuboi, M. Tsuji, Appl. Surf. Sci. **254**, 5224 (2008).

[25] R. Zamiri, B. Z. Azmi, M. Darroudi, A.R. Sadrolhosseini, M.S. Husin, A.W. Zaidan, M. A. Mahdi, Appl. Phys. A. **102**, 189 (2011).

[26] F. Mafune, J. Kohno, Y. Takeda, T.Kondow and H. Sawabe, J. Phys. Chem. B **104**, 9111(2000).

[27] W. T. Nichols1, T. Sasaki, N. Koshizaki, J. Appl. Phys. **100**, 114913 (2006).

[28] G. Yang, Laser ablation in liquids, 1nd edn. (Pan Stanford Publishing, Singapore, 2012), 340-345.

[29] A.R. Sadrolhosseini, A.S.M. Noor, K. Shameli, G. Mamdoohi, M. M. Moksin, M. A. Mahdi, Journal of Materials Research, **28**, 2629 (2013).

[30] S. Vijay, A. Raykar and K. Singh, Journal of Thermodynamics, **2011**, 464368 (2011).

[31] K.K. Kraning, J. Appl. Physiol. **35**, 281(1973).

[32] I. Tanasawa, N. Katsuta, S. Kenkyu; **24**, 440 (1972).

[33] A. Yoshida, K. Kagata, T.Yamada, Int J Thermophys, **31**, 2019 (2010).

[34] G. G. Ju´arez, M. Vargas-Luna, T C´ordova, J. B. Varela, J. J. Bernal-Alvarado, M. Sosa, Physiol. Meas. **23**, 521 (2002).

[35] A.R. Sadrolhosseini, A.S.M. Noor ASM, K. Shameli, A. Kharazmi, N.M. Huang, M. A. Mahdi, Journal of Nanomaterials, **2013**, 986764 (2013).

[36] L. Qiu, F. Liu, L. Zhao, W. Yang, J. Yao, Langmuir, **22**, 4480 (2006).

[37] A. I. Roucoux, J. Schulz, P. Henri, Chem. Rev. **102**, 3757 (2002).

[38] R. Zamiri, A. Zakaria, H. A. Ahangar, A.R. Sadrolhosseini, M. A. Mahdi, Int. J. Mol. Sci. **11**, 4764 (2010).

[39] N. M. Huang, H. N. Lim, C.H. Chia, M. A. Yarmo, M. R. Muhamad, International Journal of Nanomedicine, **6**, 3443 (2011).

[40] D. L. Pavia, G. M. Lampman, G. S. Kriz, Introduction to spectroscopy, 1nd edn. (Thomson Learning, Australia, 2001) pp. 40-140.

[41] O. Delgado-Vasallo, E. Marin, Journal of Phys. D: Applied Physics, **32**, 593 (1999).